Near-field properties of diffraction through a circular subwavelength-size aperture*

Wang Zheng-Ling(王正岭)[a)b)†], Zhou Ming(周 明)[a)‡], Gao Chuan-Yu(高传玉)[a)], and Zhang Wei(张 伟)[a)]

[a)] *School of Materials Science and Engineering, Jiangsu University, Zhenjiang* 212013, *China*
[b)] *Department of Physics, Jiangsu University, Zhenjiang* 212013, *China*

(Received 14 November 2011; revised manuscript received 5 December 2011)

Analytical nonparaxial vectorial electric field expressions for both Gaussian beams and plane waves diffracted through a circular aperture are derived by using the vector plane angular spectrum method for the first time, which is suitable for the subwavelength aperture and the near-field region. The transverse properties of intensity distributions and their evolutions with the propagating distance, and the power transmission functions for diffracted fields containing the whole field, the evanescent field and the propagating field are investigated in detail, which is helpful for understanding the relationship between evanescent and propagating components in the near-field region and can be applied to apertured near-field scanning optical microscopy.

Keywords: analytical expressions, diffraction, circular subwavelength aperture, near-field properties

PACS: 42.25.Fx, 42.25.Bs, 42.25.–p **DOI:** 10.1088/1674-1056/21/6/064202

1. Introduction

The electromagnetic fields passing through a circular aperture have been investigated for a long time,[1−9] and the incident light model of a Gaussian beam in transverse distribution is generally studied,[6,7] while the plane wave has also been taken into consideration for simpler incident light models.[8,9] Recently, more accurate solutions to the electromagnetic equations for aperture diffraction have received much attention. Generally, the scalar representation from paraxial approximation cannot satisfy the Maxwell equations and cannot be used in a large divergent beam or a small beam spot size comparable to the wavelength.

To overcome this drawback, the vector representation based on the nonparaxial framework has been developed to resolve the Maxwell equations, such as the vector angular spectrum method,[10,11] the Hertz vector diffraction theory,[3,7−9] the vectorial Rayleigh diffraction, and so on.[6,12] The vector angular spectrum method has received more and more attention recently because it is a useful and convenient tool to resolve the propagation of a light field[10,13−20] and the far-field diffraction of nonparaxial Gaussian beams at a circular aperture.[11] At the same time, the Hertz vector diffraction theory has also been taken as an important method to study circular aperture diffraction.[3,7−9] In 2005, Guha and Gillen[8] derived integral expressions for the electric and magnetic field components of light within and beyond an apertured plane for an incident plane wave by using the nonparaxial vector diffraction theory. In 2009, Gillen *et al.*[7] investigated a focused TEM_{00} Gaussian light field passing through a circular aperture by using the Hertz vector diffraction theory. In addition, in 2003, Lü and Duan[6] investigated the nonparaxial propagation of vectorial Gaussian beams diffracted at a circular aperture by using the vectorial Rayleigh diffraction integral. And in 2004, Gillen and Guha[12] also used the complete Rayleigh–Sommerfeld method to discuss the model and propagation of near-field diffraction patterns.

Moreover, as is well known, the diffraction of light at an aperture with a radius comparable to or smaller than the wavelength λ of light is a challenging researching topic and must be described by the vector theory, in which the light field is restricted to about a wavelength size scale, and it is composed of an evanescent field and a propagating wave in the near-field. So

*Project supported by the National Natural Science Foundation of China (Grant No. 50975128), the National Key Basic Research Program of China (Grant No. 2011CB013004), the Natural Science Foundation of Jiangsu Province, China (Grant No. BK2011462), the National Science Foundation for Postdoctoral Scientists of China (Grant No. 20100481093), and Jiangsu Provincial Planned Projects for Postdoctoral Research Funds, China (Grant No. 0902028C).

†Corresponding author. E-mail: zlwang@ujs.edu.cn
‡Corresponding author. E-mail: zm2109@126.com

© 2012 Chinese Physical Society and IOP Publishing Ltd

far, the analytical nonparaxial vector expression for the diffraction through the circular aperture with subwavelength size (several 0.1λ) in the near-field (several 0.1λ) and the properties of the evolving evanescent field and the propagating wave, as well as their relationship, have not been achieved completely. The diffraction through a circular subwavelength-size aperture in the near-field is important for apertured near-field scanning optical microscopy using a near-field optical probe with a subwavelength-sized opening, which has already become a widely used tool for optical imaging with several 10-nm spatial resolution. Therefore, it would be interesting and worthwhile to study the diffraction through a circular subwavelength-size aperture.

In this paper, analytical nonparaxial vectorial electric field expressions in the form of convergent series and the power transmission functions and their prosperities of the diffraction through a circular subwavelength-size aperture are investigated based on the vector plane angular spectrum. The rest of the present paper is organized as follows. In Section 2, we derive the analytical expression of a nonparaxial electric field diffracted through a circular aperture for both Gaussian beams and plane waves. In Section 3, we analyse and discuss the diffracted intensity distribution prosperities in the near-field. In Section 4, we study the power transmission functions in the near- (and far-) field. Some main results and conclusions are summarized in Section 5 finally.

2. Analytical expressions of electric fields diffracted through a circular aperture

A Gaussian beam with polarization in the x direction propagates along the z axis, and a circular aperture of radius R is located at the plane $z = 0$. The electric fields just at the aperture can be expressed as[11]

$$E_x(x_0, y_0, 0) = t(x_0, y_0) \exp\Big(-\frac{x_0^2 + y_0^2}{w^2}\Big), \quad (1a)$$

$$E_y(x_0, y_0, 0) = 0, \quad (1b)$$

where w is the beam waist, and the window function of the circular aperture $t(x_0, y_0) = 1$ as $x_0^2 + y_0^2 \le R^2$, and $t(x_0, y_0) = 0$ otherwise.

According to the angular spectrum representation, any electric field can be expanded into an angular spectrum of plane waves in the region $z \ge 0$, where in the region $p^2 + q^2 \le 1$, every plane wave is homogeneous, while in the region $p^2 + q^2 > 1$ every plane wave decays exponentially along z. Note that p and q are two coordinate components in the angular spectrum Cartesian coordinate system here. Performing a coordinate transformation from the Cartesian coordinate system (x_0, y_0) to the polar one (ρ, θ) with $\rho^2 = x_0^2 + y_0^2$ and also performing a coordinate transformation from the Cartesian coordinate system (p, q) to the polar one (r, α) with $r^2 = p^2 + q^2$, we can derive the double integrals of evanescent electric field amplitudes in the region $p^2 + q^2 > 1$ (that is $r > 1$) as follows:[11,14–20]

$$E_x^{\rm ev}(x, y, z) = k^2 \int_1^\infty \int_0^R \mathrm{J}_0(k\rho r)\mathrm{J}_0\big(kr\sqrt{x^2 + y^2}\big) \exp\Big(-\frac{\rho^2}{w^2}\Big) \exp\big(-kz\sqrt{r^2 - 1}\big) r\rho \,\mathrm{d}\rho \,\mathrm{d}r, \quad (2a)$$

$$E_y^{\rm ev}(x, y, z) = 0, \quad (2b)$$

$$E_z^{\rm ev}(x, y, z) = \frac{2\pi}{\lambda^2} \int_1^\infty \int_0^R \frac{r^2\rho}{\sqrt{r^2 - 1}} \mathrm{J}_0(k\rho r)\mathrm{J}_1\big(kr\sqrt{x^2 + y^2}\big) \sin\Big(\arctan\frac{x}{y}\Big) \exp\Big(-\frac{\rho^2}{w^2}\Big) \exp\big(-kz\sqrt{r^2 - 1}\big) \,\mathrm{d}\rho \,\mathrm{d}r, \quad (2c)$$

where $k = 2\pi/\lambda$ is the wave number, and λ is the wavelength in the medium. Similarly, in the region $p^2 + q^2 \le 1$ (that is $r \le 1$), we can derive the double integrals of the propagating electric field amplitudes as follows:[11,14–20]

$$E_x^{\rm pr}(x, y, z) = k^2 \int_0^1 \int_0^R \mathrm{J}_0(k\rho r)\mathrm{J}_0\big(kr\sqrt{x^2 + y^2}\big) \exp\Big(-\frac{\rho^2}{w^2}\Big) \exp\big(\mathrm{i}\, kz\sqrt{1 - r^2}\big) r\rho \,\mathrm{d}\rho \,\mathrm{d}r, \quad (3a)$$

$$E_y^{\rm pr}(x, y, z) = 0, \quad (3b)$$

$$E_z^{\rm pr}(x, y, z) = \mathrm{i}\,\frac{2\pi}{\lambda^2} \int_0^1 \int_0^R \frac{r^2\rho}{\sqrt{1 - r^2}} \mathrm{J}_0(k\rho r)\mathrm{J}_1\big(kr\sqrt{x^2 + y^2}\big) \sin\Big(\arctan\frac{x}{y}\Big) \exp\Big(-\frac{\rho^2}{w^2}\Big) \exp\big(\mathrm{i}\, kz\sqrt{1 - r^2}\big) \,\mathrm{d}\rho \,\mathrm{d}r. \quad (3c)$$

In Eqs. (2) and (3), $\mathrm{J}_l(x)$ is the first kind l-th order Bessel function, and $\mathrm{J}_l(x)$ can be expanded into the series as follows:

$$\mathrm{J}_l(x) = \sum_{m=0}^{\infty} \frac{(-1)^m x^{2m+l}}{m!(m + l)!2^{2m+l}}. \quad (4)$$

Substituting Eq. (4) into Eq. (2), then applying Newton's Binomial Theorem, we can derive the expressions of the evanescent electric field amplitudes in the form of series as follows:

$$E_x^{\rm ev}(x,y,z) = \sum_{m=0}^{\infty}\sum_{n=0}^{\infty}\sum_{l=0}^{m+n}\Big\{\frac{(-1)^{m+m}k^{2m+2n-2l}w^{2m+2}(2l+1)!}{(m!)^2(n!)^2 l!\,2^{2m+2n+1}} \times (m+n)(m+n-1)\cdot(m+n-l+1)\cdot\Big[m!-\Gamma\Big(m+1,\frac{R^2}{w^2}\Big)\Big]\cdot\frac{(x^2+y^2)^n}{z^{2l+2}}\Big\}, \tag{5a}$$

$$E_y^{\rm ev}(x,y,z) = 0, \tag{5b}$$

$$E_z^{\rm ev}(x,y,z) = \frac{1}{2\pi}\sin(\arctan\frac{x}{y})\sum_{m=0}^{\infty}\sum_{n=0}^{\infty}\sum_{l=0}^{m+n+1}\Big\{\frac{(-1)^{m+m}k^{2m+2n-2l+2}w^{2m+2}(2l)!}{(m!)^2 n!\,(n+1)!\,l!\,2^{2m+2n+2}} \times (m+n+1)(m+n)\cdot(m+n-l+2)\cdot\Big[m!-\Gamma\Big(m+1,\frac{R^2}{w^2}\Big)\Big]\cdot\frac{(x^2+y^2)^{n+1/2}}{z^{2l+1}}\Big\}, \tag{5c}$$

where $\Gamma(\cdot,\cdot)$ is the incomplete gamma function. Similarly, substituting Eq. (4) into Eq. (3), we can derive the expressions of the propagating electric field amplitudes in the form of series as follows:

$$E_x^{\rm pr}(x,y,z) = \sum_{m=0}^{\infty}\sum_{n=0}^{\infty}\sum_{l=0}^{m+n}\Big\{\frac{(-1)^{m+m+1}k^{2m+2n-2l}w^{2m+2}(m+n)(m+n-1)\cdot(m+n-l+1)}{(m!)^2(n!)^2 l!\,2^{2m+2n+1}} \times\Big[!-\Gamma\Big(m+1,\frac{R^2}{w^2}\Big)\Big]\cdot\Big[(2l+1)!-\Gamma(2l+2,-\mathrm{i}\,kz)\Big]\cdot\frac{(x^2+y^2)^n}{z^{2l+2}}\Big\}, \tag{6a}$$

$$E_y^{\rm pr}(x,y,z) = 0, \tag{6b}$$

$$E_z^{\rm pr}(x,y,z) = \frac{1}{2\pi}\sin\Big(\arctan\frac{x}{y}\Big)\sum_{m=0}^{\infty}\sum_{n=0}^{\infty}\sum_{l=0}^{m+n+1}\Big\{\frac{(-1)^{m+m+1}k^{2m+2n-2l+2}w^{2m+2}}{(m!)^2 n!\,(n+1)!l!2^{2m+2n+2}}\Big[m!-\Gamma\Big(m+1,\frac{R^2}{w^2}\Big)\Big] \times(m+n+1)(m+n)\cdot(m+n-l+2)\cdot[(2l)!-\Gamma(2l+1,-\mathrm{i}\,kz)]\cdot\frac{(x^2+y^2)^{n+1/2}}{z^{2l+1}}\Big\}. \tag{6c}$$

Equations (5) and (6) are the basic analytical nonparaxial vector electric field expressions of the Gaussian beam diffracted through the circular aperture, respectively. For mathematical simplicity, plane waves have been chosen as the incident light for various vector diffraction theories.[8,9] When the aperture radius R is much smaller than the beam width w in the aperture plane, a virtually uniform field within the aperture can be produced and they can be thought as the plane wave. Since the radius R of the circular aperture considered in this paper is very small (a fraction of wavelength λ) in the near-field region, the variation between the intensity in the centre of the aperture and one at the edge of the aperture is very small. For example, this variation of the intensity is about 0.02% for a value of $R/w = 0.01$. Thus the incident Gaussian beam in the aperture region is virtually uniform, and calculations can be thought as a plane wave at the circular aperture. Therefore, if we take the plane wave with the amplitude of 1 and a polarization in the x direction as the incident light in Eq. (1), we can derive the expressions of evanescent electric field amplitudes for the plane wave as follows:

$$E_x^{\rm ev}(x,y,z) = kR\int_1^{\infty}\mathrm{J}_1(kRr)\mathrm{J}_0(kr\sqrt{x^2+y^2})\exp(-kz\sqrt{r^2-1})\,\mathrm{d}r = \sum_{m=0}^{\infty}\sum_{n=0}^{\infty}\sum_{l=0}^{m+n}\Big\{\frac{(-1)^{m+n}k^{2m+2n-2l}R^{2m+2}(2l+1)!}{m!(m+1)!(n!)^2 l!2^{2m+2n+1}} \times(m+n)(m+n-1)\cdot(m+n-l+1)\cdot\frac{(x^2+y^2)^n}{z^{2l+2}}\Big\}, \tag{7a}$$

$$E_y^{ev}(x,y,z) = 0, \tag{7b}$$

$$E_z^{\rm ev}(x,y,z) = \frac{R}{\lambda}\int_1^{\infty}\frac{r}{\sqrt{r^2-1}}\mathrm{J}_1(kRr)\mathrm{J}_1(kr\sqrt{x^2+y^2})\sin\Big(\arctan\frac{x}{y}\Big)\exp(-kz\sqrt{r^2-1})\,\mathrm{d}r = \frac{1}{2\pi}\sin\Big(\arctan\frac{x}{y}\Big)\sum_{m=0}^{\infty}\sum_{n=0}^{\infty}\sum_{l=0}^{m+n+1}\Big\{\frac{(-1)^{m+n}k^{2m+2n-2l+2}R^{2m+2}(2l)!}{m!(m+1)!n!\,(n+1)!l!2^{2m+2n+2}} \times(m+n+1)(m+n)\cdot(m+n-l+2)\cdot\frac{(x^2+y^2)^{n+1/2}}{z^{2l+1}}\Big\}. \tag{7c}$$

Similarly we can also derive the expressions of propagating electric field amplitudes for the plane wave as

follows:

$$E_x^{\rm pr}(x,y,z) = kR\int_0^1 {\rm J}_1(kRr){\rm J}_0(kr\sqrt{x^2+y^2})\exp({\rm i}\,kz\sqrt{1-r^2})\,{\rm d}r$$
$$= \sum_{m=0}^{\infty}\sum_{n=0}^{\infty}\sum_{l=0}^{m+n}\Big\{\frac{(-1)^{m+n+1}k^{2m+2n-2l}R^{2m+2}}{m!(m+1)!(n!)^2 l!2^{2m+2n+1}}[(2l+1)!-\Gamma(2l+2,-{\rm i}\,kz)]$$
$$\times(m+n)(m+n-1)\cdots(m+n-l+1)\cdot\frac{(x^2+y^2)^n}{z^{2l+2}}\Big\}, \tag{8a}$$

$$E_y^{pr}(x,y,z) = 0, \tag{8b}$$

$$E_z^{\rm pr}(x,y,z) = {\rm i}\,\frac{R}{\lambda}\int_0^1 \frac{r}{\sqrt{1-r^2}}{\rm J}_1(kRr){\rm J}_1(kr\sqrt{x^2+y^2})\sin\Big(\arctan\frac{x}{y}\Big)\exp({\rm i}\,kz\sqrt{1-r^2})\,{\rm d}r$$
$$= \frac{1}{2\pi}\sin\Big(\arctan\frac{x}{y}\Big)\sum_{m=0}^{\infty}\sum_{n=0}^{\infty}\sum_{l=0}^{m+n+1}\Big\{\frac{(-1)^{m+n+1}k^{2m+2n-2l+2}R^{2m+2}}{m!(m+1)!n!(n+1)!l!2^{2m+2n+2}}[(2l)!-\Gamma(2l+1,-{\rm i}\,kz)]$$
$$\times(m+n+1)(m+n)\cdot(m+n-l+2)\cdot\frac{(x^2+y^2)^{n+1/2}}{z^{2l+1}}\Big\}. \tag{8c}$$

Equations (7) and (8) are the basic analytical non-paraxial vector electric field expressions of plane waves diffracted through the aperture respectively.

We can find from Eqs. (2)–(8) that the diffracted electric fields contain an evanescent electric field and a propagating electric field, and the whole electric field can be decomposed into $E_x^{\rm wh}$, $E_y^{\rm wh}$, and $E_z^{\rm wh}$ in the spatial domain, and they can be given by

$$E_x^{\rm wh}(x,y,z) = E_x^{\rm ev}(x,y,z) + E_x^{\rm pr}(x,y,z), \tag{9a}$$
$$E_y^{\rm wh}(x,y,z) = 0, \tag{9b}$$
$$E_z^{\rm wh}(x,y,z) = E_z^{\rm ev}(x,y,z) + E_z^{\rm pr}(x,y,z). \tag{9c}$$

According to Eqs. (9), the whole electric intensity can be given by

$$I(x,y,z) = I_x^{\rm wh}(x,y,z) + I_y^{\rm wh}(x,y,z) + I_z^{\rm wh}(x,y,z), \tag{10}$$

where

$$I_x^{\rm wh}(x,y,z) = |E_x^{\rm wh}(x,y,z)|^2$$
$$= I_x^{\rm ev}(x,y,z) + I_x^{\rm pr}(x,y,z) + I_x^{\rm co}(x,y,z), \tag{11a}$$
$$I_y^{\rm wh}(x,y,z) = 0, \tag{11b}$$
$$I_z^{\rm wh}(x,y,z) = |E_z^{\rm wh}(x,y,z)|^2$$
$$= I_z^{\rm ev}(x,y,z) + I_z^{\rm pr}(x,y,z) + I_z^{\rm co}(x,y,z) \tag{11c}$$

with

$$I_x^{\rm ev}(x,y,z) = |E_x^{\rm ev}(x,y,z)|^2, \tag{12a}$$
$$I_x^{\rm pr}(x,y,z) = |E_x^{\rm pr}(x,y,z)|^2, \tag{12b}$$
$$I_x^{\rm co}(x,y,z) = [E_x^{\rm ev}(x,y,z)]^*\cdot E_x^{\rm pr}(x,y,z) + E_x^{\rm ev}(x,y,z)\cdot[E_x^{\rm pr}(x,y,z)]^*, \tag{12c}$$
$$I_z^{\rm ev}(x,y,z) = |E_z^{\rm ev}(x,y,z)|^2, \tag{12d}$$
$$I_z^{\rm pr}(x,y,z) = |E_z^{\rm pr}(x,y,z)|^2, \tag{12e}$$
$$I_z^{\rm co}(x,y,z) = [E_z^{\rm ev}(x,y,z)]^*\cdot E_z^{\rm pr}(x,y,z) + E_z^{\rm ev}(x,y,z)\cdot[E_z^{\rm pr}(x,y,z)]^*. \tag{12f}$$

Here, $I_x^{\rm ev}(x,y,z)$, $I_x^{\rm pr}(x,y,z)$, and $I_x^{\rm co}(x,y,z)$ represent the evanescent field intensities, the intensity of the propagating field, and the coherence intensity of the evanescent and propagating fields for the x polarization, respectively, while $I_z^{\rm ev}(x,y,z)$, $I_z^{\rm pr}(x,y,z)$, and $I_z^{\rm co}(x,y,z)$ represent the evanescent field intensities, the intensity of the propagating field, and the coherence intensity of the evanescent and propagating fields for the z polarization, respectively.

3. Intensity distribution properties

We can find from Eqs. (5)–(8) that the analytical electric field expressions for both the Gaussian beam and the plane wave diffracted through the circular aperture can be derived without making any approximations, which allows us to investigate them near the circular aperture. And all the above presented series are from the expansion of Bessel functions and Newton's Binomial Theorem, and they are alternating and absolutely convergent. For the convenience and the accuracy of calculation, the electric field expressions of the direct numerical integration for the plane waves in Eqs. (7) and (8) are chosen in the following discussion. We can also find from Eqs. (7a) and (7c) that the evanescent fields have no limitation at $z = 0$ as $r \to \infty$, so the evanescent fields are discontinuous in the aperture plane. Here we will discuss evanescent fields from a small propagating distance, such as $z \geq 0.001\lambda$. Meanwhile, we can find from

Eqs. (8a) and (8c) that propagating fields are continuous in the aperture plane and we can discuss their properties from $z \geq 0$.

3.1. Evolution of the on-axis intensity of the x polarization along z

According to Eqs. (7)–(12), the dependences of the normalized intensity (we have supposed that the amplitude of the incident plane wave is 1 throughout this paper) of the x polarization on z as $x = y = 0$ are calculated for different values of aperture radius R and the results are shown in Figs. 1–4. Figure 1 shows the evolutions of the normalized intensity of the evanescent field $I_x^{\rm ev}(0, 0, z)$ along z for different values of R. We can find from Fig. 1 that $I_x^{\rm ev}(0, 0, z)$ will decrease rapidly with the increase of z, and the attenuation distance is very small and typically smaller than 0.3λ. The curve in Fig. 1 will become steady with the increase of R, and the value of $I_x^{\rm ev}(0, 0, z)$ will increase with the increase of R for the same z in Fig. 1(a), for example, the values of $I_x^{\rm ev}(0, 0, z)$ are 0.09, 0.3, 0.44, 0.52 for $R = 0.02\lambda$, 0.04λ, 0.06λ, 0.08λ respectively as $z = 0.02\lambda$. $I_x^{\rm ev}(0, 0, z)$ will decrease to 0 as $R \geq 0.35\lambda$ for any z, that is to say the on-axis evanescent field exists only under the condition of the very small aperture radius $R(< 0.35\lambda)$.

Figure 2 shows the evolution of the normalized on-axis intensity of the propagating field $I_x^{\rm pr}(0, 0, z)$ along z for different values of R. We can find from Fig. 2 that $I_x^{\rm pr}(0, 0, z)$ will decrease with the increase of z for small R ($R < 0.6\lambda$ in Fig. 2(a)) and $I_x^{\rm pr}(0, 0, z)$ will increase with the increase of R for the same value of z. However, the situation will change when R is larger than 0.6λ. The intensity will first increase to the maximum then decrease with the increase of z as $0.6\lambda < R < 1.0\lambda$. So the intensity will oscillate with the increase of z as $R > 0.6\lambda$. The number of on-axis intensity oscillations will be equal to R/λ.[7,8] We can find from Fig. 2 that the maximal value of $I_x^{\rm pr}(0, 0, z)$ will increase with the increase of R, and maximal values are 2.77, 3.29, and 3.57 as

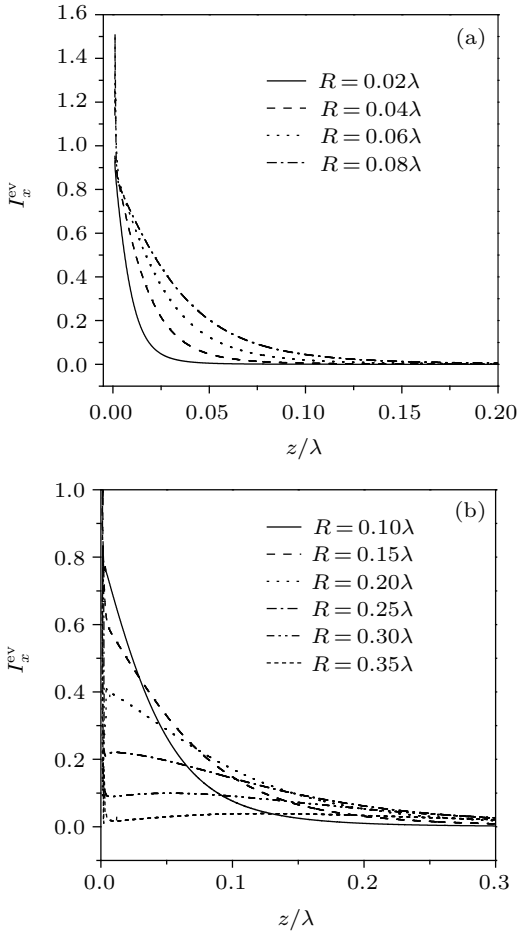


Fig. 1. Evolutions of the normalized on-axis intensity of the evanescent field of the x polarization $I_x^{\rm ev}(0, 0, z)$ along z for different values of R.

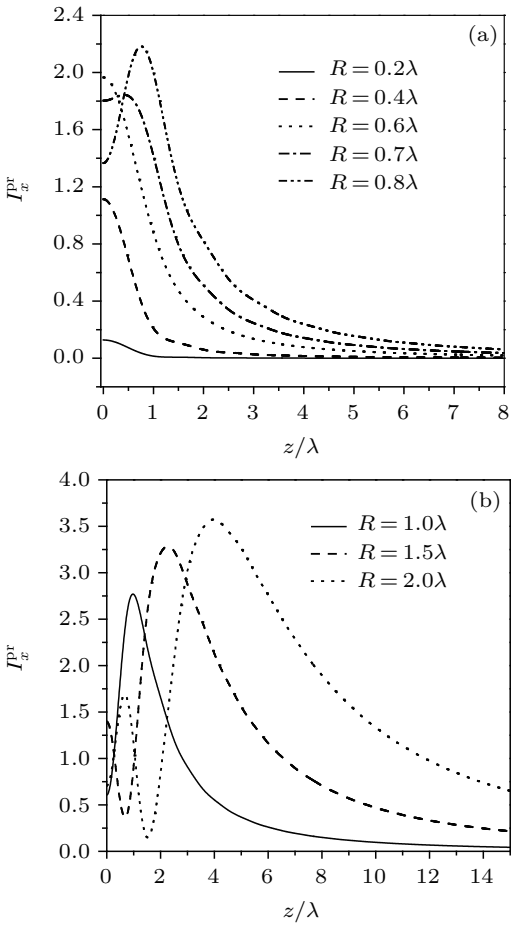


Fig. 2. Evolutions of the normalized on-axis intensity of the propagating field $I_x^{\rm pr}(0, 0, z)$ along z for different values of R.

$R = 1.0\lambda$, 1.5λ, and 2.0λ respectively, and will be located at a position of $z \approx R^2/\lambda$, which is similar to the results from Refs. [7] and [8]. And $I_x^{\rm pr}(0,\,0\,,z)$ can propagate over a larger distance z with the increase of R.

Figure 3 shows the evolutions of the normalized on-axis intensity of the coherent field $I_x^{\rm co}(0,0,z)$ along z for different values of R. $I_x^{\rm co}(x,y,z)$ comes from the coherence of evanescent and propagating fields, and $I_x^{\rm co}(0,0,z)$ will be oscillatory and decrease to 0 with the increase of z. It is obvious that the normalized intensity of the coherent field plays an important role in modulating the whole intensity in the near-field.

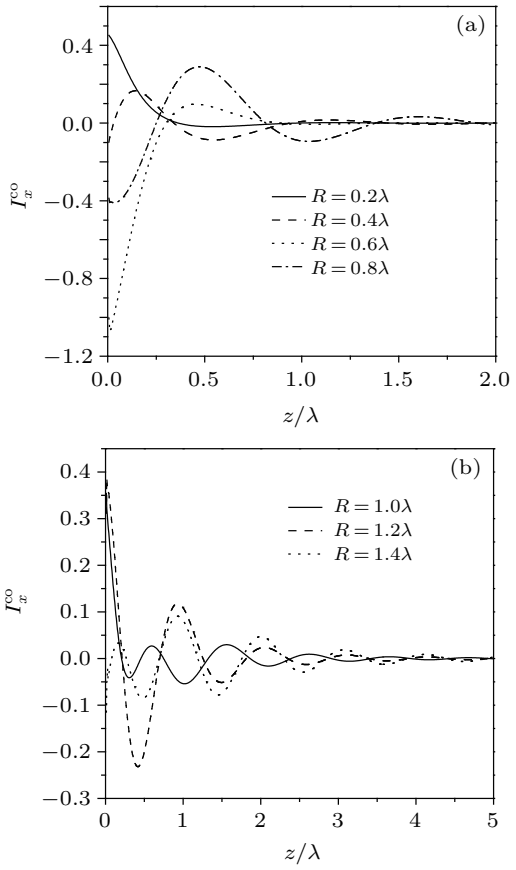


Fig. 3. Evolutions of the normalized on-axis intensity of the coherent field $I_x^{\rm co}(0,\,0\,,z)$ along z for different values of R.

Figure 4 shows the evolutions of the normalized whole on-axis intensity $I_x^{\rm wh}(0,0,z)$ along z for different values of R. We can find from Fig. 4(a) that $I_x^{\rm wh}(0,0,z)$ will decrease with the increase of z for small value of R (for example, $R \leq 0.2\lambda$) and the intensity will increase with the increase of R for the same value of z. And the intensity will first increase to a maximum then decrease with the increase of z as $0.3\lambda < R < 0.75\lambda$. We can also find from Fig. 4 that $I_x^{\rm wh}(0,0,z)$ is similar to $I_x^{\rm ev}(0,0,z)$ for very small values of R (for example, $R << 0.1\lambda$), while $I_x^{\rm wh}(0,\,0\,,z)$ is the same as $I_x^{\rm pr}(0,0,z)$ for very large values of R and a certain larger distance z, and we can think that $I_x^{\rm wh}(0,0,z)$ and $I_x^{\rm ev}(0,0,z)$ are the same for $R = 0.75\lambda$ and $z > 1.5\lambda$ as well as $R = 1.0\lambda$ and $z > 1.2\lambda$ in Fig. 4(b). When R ranges from 0.1λ to 1.0λ, the whole intensity is complicated and determined by all components. Near the aperture plane ($z \to 0$) the central whole intensity is similar to the normalized incident intensity value 1, while the maximal values of the whole intensity at the z axis ($z > 0$) will be larger than 1 and increase with the increase of R.

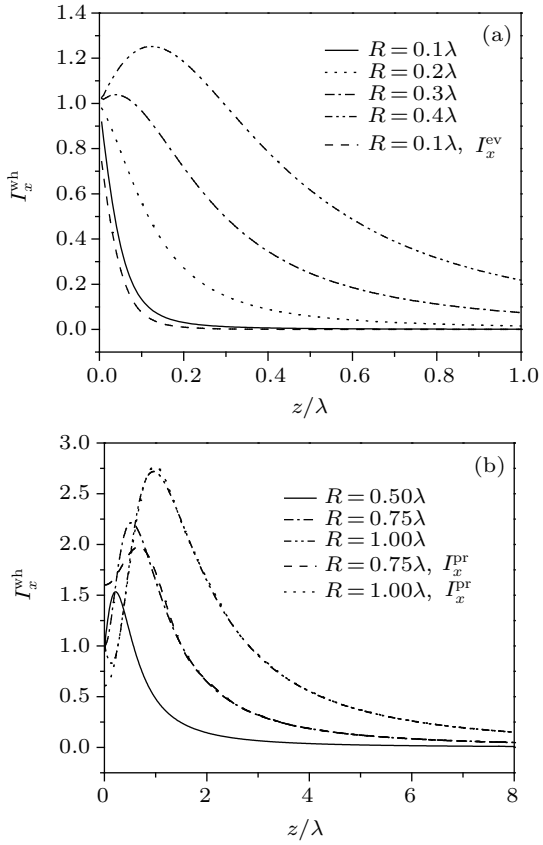


Fig. 4. Evolutions of the normalized whole on-axis intensity $I_x^{\rm wh}(0,0,z)$ along z for different values of R.

Figure 5 shows the dependences of the ratio of $I_x^{\rm pr}(0,\,0\,,z)$ to $I_x^{\rm ev}(0,\,0\,,z)$ on z for different values of R. We can find from Fig. 5 that the ratio will increase with the increase of z for a given value of R and the ratio will also increase with the increase of R for the same value of z. The ratio is smaller than 1 as $z < 0.1\lambda$ and $R \leq 0.2\lambda$, which means the evanescent field plays a key role only for small radius (for example $R \leq 0.2\lambda$) and in the near-field region (for example, a fraction of wavelength λ). When the radius R becomes large, $I_x^{\rm pr}(0,0,z)$ will be much larger than $I_x^{\rm ev}(0,0,z)$, and the propagating field plays a key role for a large radius R. For example, $I_x^{\rm pr}(0,0,z)$ is about 5 times $I_x^{\rm ev}(0,0,z)$ for $R = 0.3\lambda$ as $0.01\lambda < z < 0.1\lambda$, and $I_x^{\rm pr}(0,0,z)$ is about 27 times $I_x^{\rm ev}(0,0,z)$ for $R = 0.3\lambda$ as $z = 0.4\lambda$.

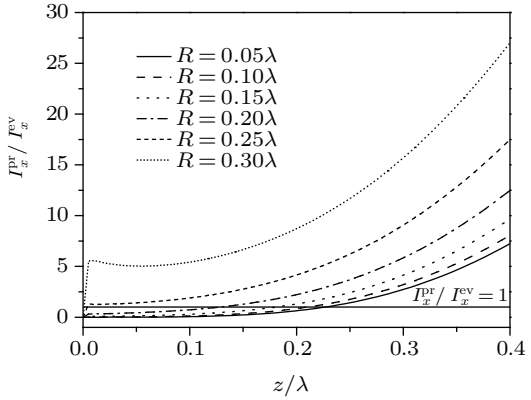


Fig. 5. Dependences of the ratio of $I_x^{\rm pr}(0,0,z)$ to $I_x^{\rm ev}(0,0,z)$ on z for different values of R.

3.2. Transverse distribution of the normalized intensity of the x polarization

We can find from Eqs. (7)–(12) that the transverse distributions of $I_x^{\rm ev}$, $I_x^{\rm pr}$, $I_x^{\rm co}$, and $I_x^{\rm wh}$ are axially symmetrical, and here we discuss only the transverse intensity of the x polarization in the x direction (taking $y = 0$). According to Eqs. (11)–(16), the normalized transverse intensities of the x polarization are calculated in the x direction ($y = 0$) for different values of R and results are shown in Figs. 6–9. Figure 6 shows the transverse distributions of the normalized intensity of the evanescent field $I_x^{\rm ev}(x, 0, z = c)$ in the x direction for different values of z and R. We can find from Fig. 6 that the transverse distributions of $I_x^{\rm ev}(x, 0, z = c)$ are different for different values of R, and values of $I_x^{\rm ev}(x, 0, z = c)$ will decrease rapidly to 0 with the increase of z. We can find from Figs. 6(c) and 6(d) that the transverse distributions will change with the increase of z for $R = 0.3\lambda$ or 0.4λ, and the dark spot in the vicinity of the centre for $R = 0.3\lambda$ as $z = 0.025\lambda$ will be converted into a light spot as $z \geq 0.075\lambda$ as well as the dark spot in the vicinity of the centre for $R = 0.4\lambda$ as $z \leq 0.15\lambda$ will be converted into a light spot as $z \geq 0.2\lambda$.

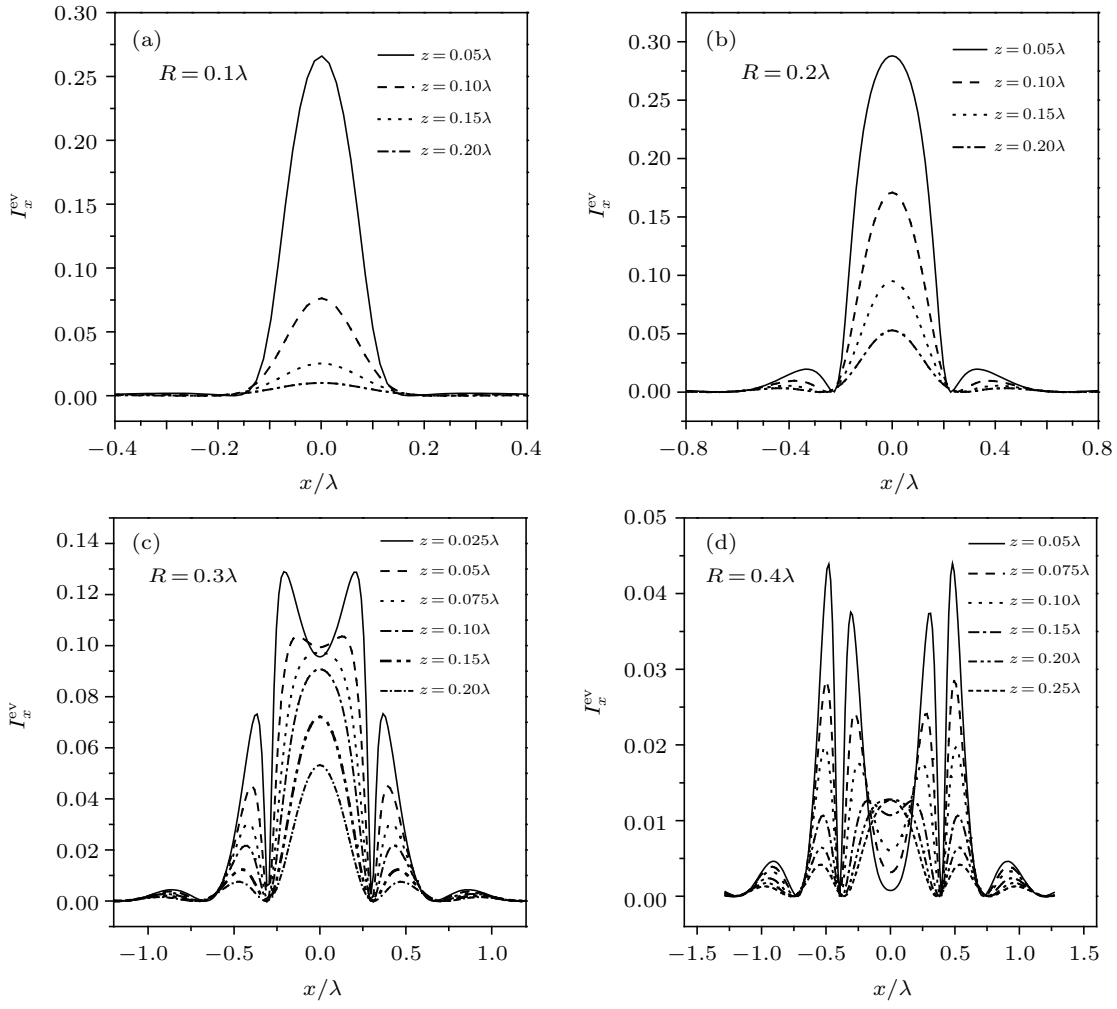


Fig. 6. Transverse distributions of the normalized intensity of the evanescent field $I_x^{\rm ev}(x, 0, z = c)$ in the x direction for different values of z and R, as indicated in each panel.

Figure 7 shows the transverse distributions of the normalized intensity of the propagating field $I_x^{\rm pr}(x, 0, z = c)$ of the x polarization in the x direction for different values of R and z. We can find from Figs. 7(a) and 7(b) that the transverse distributions of $I_x^{\rm pr}(x, 0, z = c)$ are not Gaussian distributions as $R = 0.1\lambda$, and they have maximal values in the centre and decrease to zero with the increase of x in the transverse spot. However, the oscillation of $I_x^{\rm pr}(x, 0, z = c)$ will disappear and the transverse spot will evolve into a Gaussian one with the values of R and z increasing, which can be seen in Figs. 7(c) and 7(d) as $R = 0.4\lambda$ and $z = 1.0\lambda$. It means that the transverse distribution of the normalized intensity of the propagating field will be converted from a non-Gaussian mode distribution into a Gaussian one with light propagating as $R \geq 0.4\lambda$.

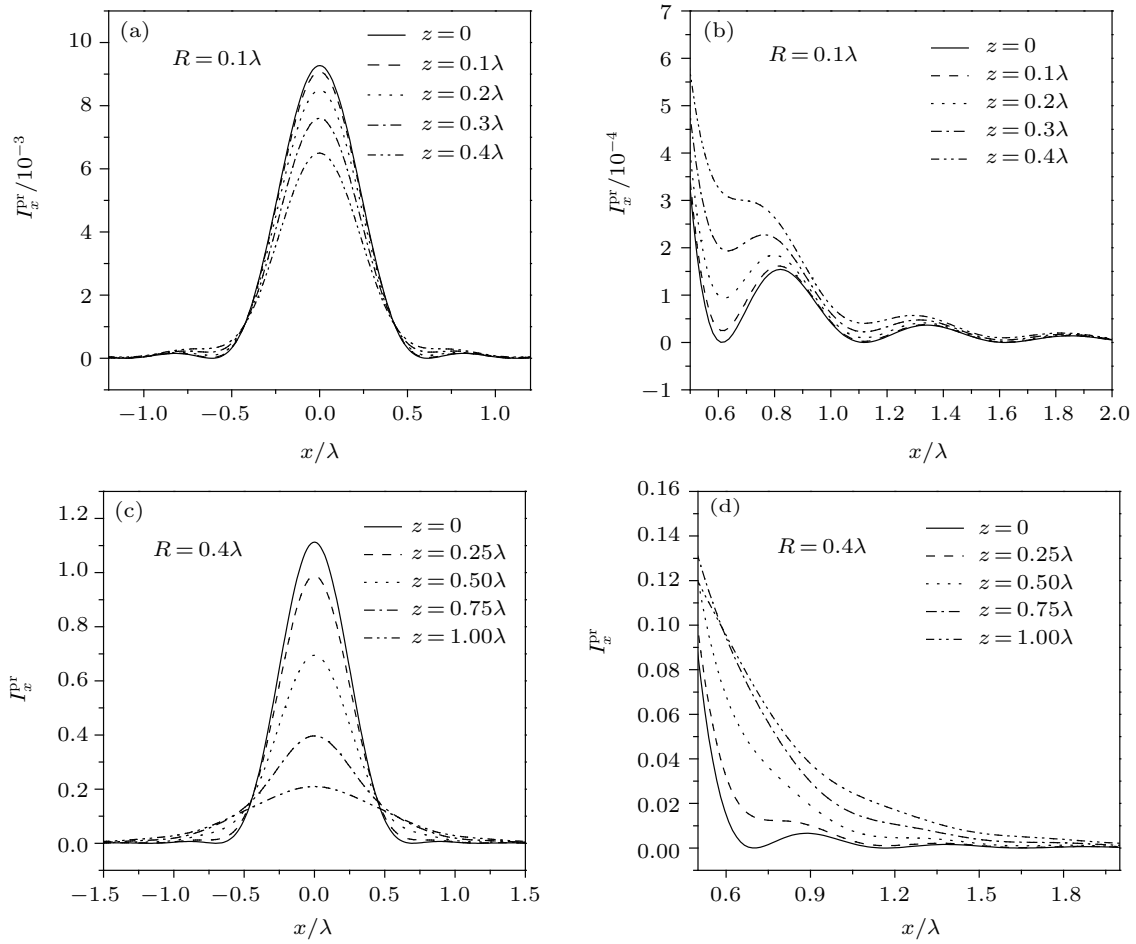


Fig. 7. Transverse distributions of the normalized intensity of the propagating field $I_x^{\rm pr}(x, 0, z = c)$ in the x direction for different values of z and R as indicated in each panel. Panel (d) is the enlarged panel (c) as $R = 0.4\lambda$.

Figure 8 shows the transverse distributions of the normalized intensity of the coherence component $I_x^{\rm co}(x, 0, z = c)$ of the x polarization in the x direction as $R = 0.1\lambda$ and $z = 0.5\lambda$, 0.75λ, 1.0λ. We can find from Fig. 8 that the transverse distributions of $I_x^{\rm co}(x, 0, z = c)$ are not Gaussian distributions, and they have maximal values in the centre and decrease to zero with the increase of x in the transverse spot. And values of $I_x^{\rm co}(x, 0, z = c)$ will also decrease to 0 with the increase of z, which is similar to the case of the evanescent field.

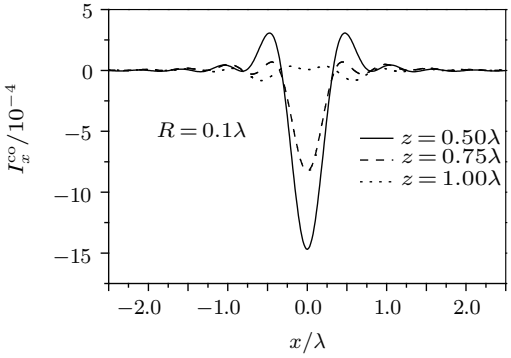


Fig. 8. Transverse distributions of the normalized intensity of the coherence component $I_x^{\rm co}(x, 0, z = c)$ of the x polarization in the x direction as $R = 0.1\lambda$ and $z = 0.5\lambda$, 0.75λ, 1.0λ.

Figure 9(a) shows the transverse distributions of the normalized intensity of the whole field $I_x^{\rm wh}(x,\,0,\,z)$ of the x polarization in the x direction as $R = 0.1\lambda$ and $z = 0.1\lambda$, 0.15λ, 0.2λ. We can find from Fig. 9(a) that the transverse distribution of $I_x^{\rm wh}(x, 0, z = c)$ can be thought as a Gaussian distribution. Figure 9(b) shows the transverse distributions of $I_x^{\rm ev}$, $I_x^{\rm pr}$, $I_x^{\rm co}$, and their overlapping $I_x^{\rm wh}$ as $R = 0.1\lambda$ and $z = 0.2\lambda$. Figure 9(c) shows the transverse distributions of $I_x^{\rm wh}$ and $I_x^{\rm pr}$ as $R = 1\lambda$ and $z = 1.0\lambda$, 1.5λ, 2.0λ. We can find from Fig. 9(c) that the transverse distributions of $I_x^{\rm wh}(x, 0, z = c)$ can be thought of as a Gaussian distribution, and $I_x^{\rm pr}$ and $I_x^{\rm wh}$ can be thought of as the same as $R = 1.0\lambda$ and $z \geq 0.2\lambda$.

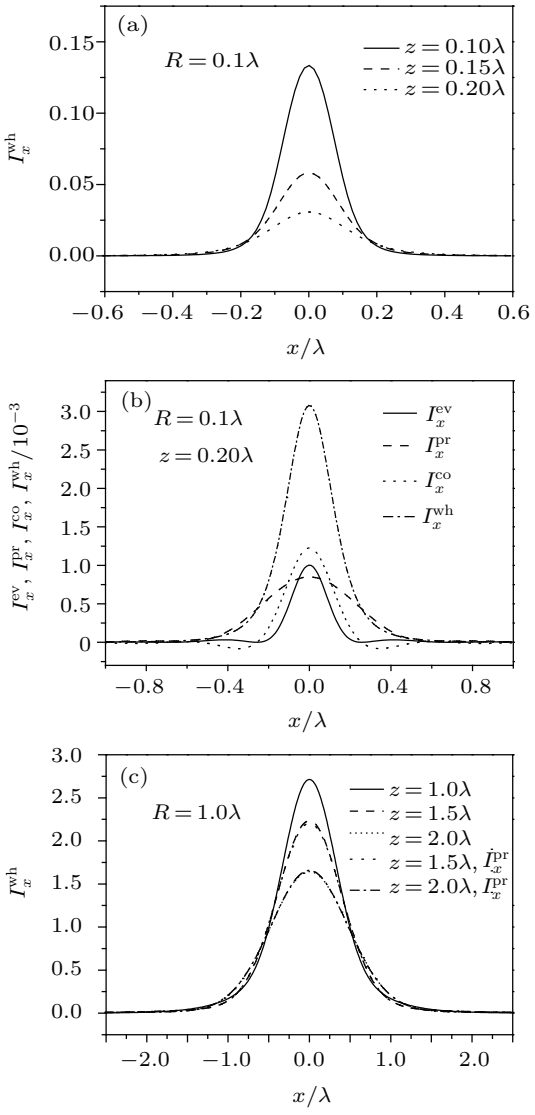


Fig. 9. (a) Transverse distributions of the normalized intensity of the whole field $I_x^{\rm wh}(x,\,0\,,z)$ of the x polarization in the x direction as $R = 0.1\lambda$ and $z = 0.1\lambda$, 0.15λ, 0.2λ; (b) the transverse distributions of $I_x^{\rm ev}$, $I_x^{\rm pr}$, $I_x^{\rm co}$, and their overlapping $I_x^{\rm wh}$ as $R = 0.1\lambda$ and $z = 0.2\lambda$; (c) the transverse distribution of $I_x^{\rm wh}$ and $I_x^{\rm pr}$ as $R = 1.0\lambda$ and $z = 1.0\lambda$, 1.5λ, 2.0λ.

3.3. Transverse distribution of the normalized intensity of the z polarization

We can find from Eqs. (7)–(12) that the transverse distributions of $I_z^{\rm ev}$, $I_z^{\rm pr}$, $I_z^{\rm co}$, and $I_z^{\rm wh}$ of the z polarization are not axially symmetric and their values are always 0 as $x = 0$, which are different from the case of the axially symmetric transverse distributions of $I_x^{\rm ev}$, $I_x^{\rm pr}$, $I_x^{\rm co}$, and $I_x^{\rm wh}$.

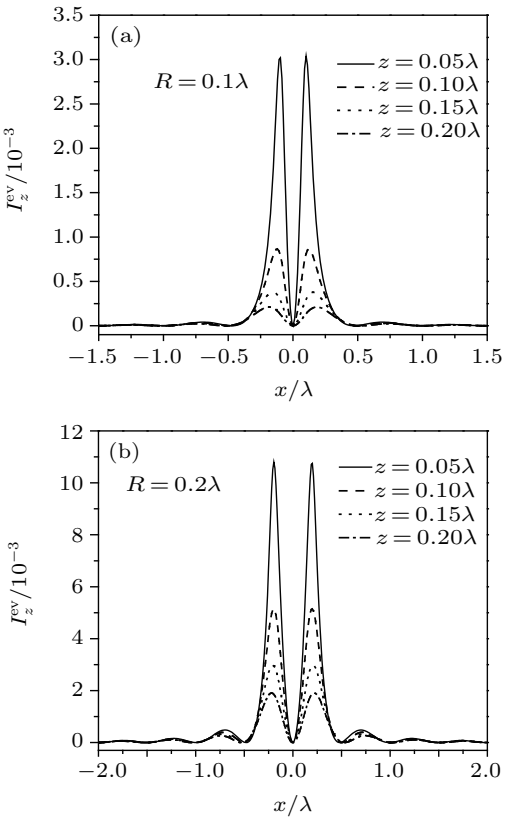


Fig. 10. Transverse distributions of the normalized intensity of the evanescent field $I_z^{\rm ev}(x, 0, z = c)$ of the z polarization for different values of z and (a) $R = 0.1\lambda$; (b) $R = 0.2\lambda$.

According to Eqs. (7)–(12), the normalized transverse intensities of the z polarization are calculated in the x direction ($y = 0$) for different values of R and the results are shown in Figs. 10–13. Figure 10 shows the transverse distributions of the normalized intensity of the evanescent field $I_z^{\rm ev}(x, 0, z = c)$ of the z polarization for different values of R and z. We can find from Fig. 10 that the transverse distributions of $I_z^{\rm ev}(x, 0, z = c)$ for different values of R are similar, and values of $I_z^{\rm ev}(x, 0, z = c)$ will decrease rapidly with the increase of z. We can find from Figs. 6 and 10 that the maximal value of $I_z^{\rm ev}(x, 0, z = c)$ is much smaller than one of $I_x^{\rm ev}(x, 0, z = c)$ for the same values of R and z. For example, maximal values of $I_x^{\rm ev}(x, 0, z = c)$ and $I_z^{\rm ev}(x, 0, z = c)$ are 0.27 and 0.003 for $R = 0.1\lambda$

and $z = 0.05\lambda$ respectively, and the difference is 90 times. The difference will decrease with the increase of R, for example, the difference is about 25 times for $R = 0.2\lambda$ and $z = 0.05\lambda$, while the difference is about 17.6 times for $R = 1.0\lambda$ and $z = 0.05\lambda$. So the maximal amplitude of intensity distribution of the evanescent field of the z polarization is much smaller than that of the x polarization and can be neglected.

Figure 11 shows the transverse distributions of the normalized intensity of the propagating field $I_z^{\rm pr}(x, 0, z = c)$ of the z polarization in the x direction for different values of R and z. We can find from Fig. 11 that the transverse distributions of $I_z^{\rm pr}(x, 0, z = c)$ are similar to each other for different values of R, and values of $I_z^{\rm pr}(x, 0, z = c)$ will decrease rapidly with the increase of z. We can find from Figs. 7 and 11 that the maximal value of $I_z^{\rm pr}(x, 0, z = c)$ is much smaller than one of $I_x^{\rm pr}(x, 0, z = c)$ for the same values of R and z. For example, maximal values of $I_x^{\rm pr}(x, 0, z = c)$ and $I_z^{\rm pr}(x, 0, z = c)$ are 0.0091 and 0.0001696 for $R = 0.1\lambda$ and $z = 0.1\lambda$ respectively, and the difference is about 53.7 times. Maximal values of $I_x^{\rm pr}(x, 0, z = c)$ and $I_z^{\rm pr}(x, 0, z = c)$ are 0.695 and 0.00607 for $R = 0.4\lambda$ and $z = 0.5\lambda$ respectively, and the difference is about 114.5 times for $R = 0.4\lambda$ and $z = 0.5\lambda$. Maximal values of $I_x^{\rm pr}(x, 0, z = c)$ and $I_z^{\rm pr}(x, 0, z = c)$ are 1.85 and 0.01 for $R = 1.0\lambda$ and $z = 0.5\lambda$, respectively, and the difference is 185 times. So the maximal amplitude of intensity distribution of the propagating field of the z polarization is much smaller than that of the x polarization and can be neglected.

Figure 12 shows the transverse distributions of the normalized intensity of the coherent field $I_z^{\rm co}(x, 0, z = c)$ of the z polarization in the x direction for different values of R and z. We can find from Fig. 12 that the transverse distributions of $I_z^{\rm co}(x, 0, z = c)$ are similar to each other for different values of R, and values of $I_z^{\rm co}(x, 0, z = c)$ will decrease rapidly with the increase of z. The maximal value of $I_z^{\rm co}(x, 0, z = c)$ is much smaller than one of $I_x^{\rm co}(x, 0, z = c)$ for the same values of R and z. So the maximal amplitude of intensity distribution of the coherent field of the z polarization is much smaller than that of the x polarization and can be neglected.

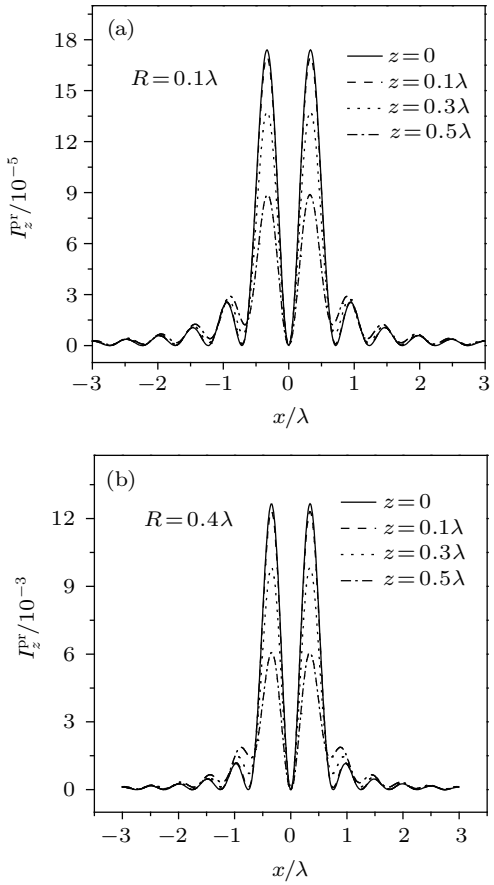


Fig. 11. Transverse distributions of the normalized intensity of the propagating field $I_z^{\rm pr}(x, 0, z = c)$ of the z polarization in the x direction for different values of R and z as indicated in the panels.

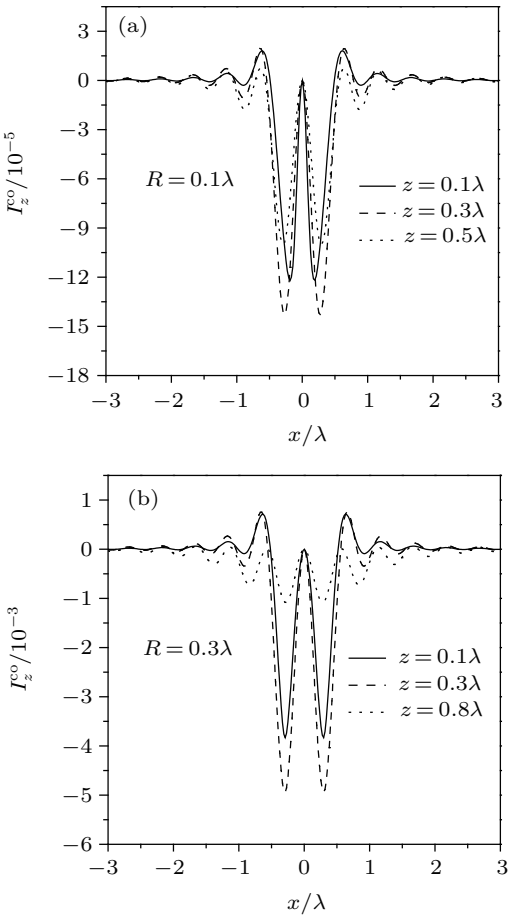


Fig. 12. Transverse distributions of the normalized intensity of the coherent field $I_z^{\rm co}(x, 0, z = c)$ of the z polarization in the x direction for different values R and z.

Figure 13(a) shows the transverse distributions of the normalized intensity of the whole field $I_z^{\rm wh}(x,0,z)$ of the z polarization in the x direction as $R=0.1\lambda$ and $z=0.1\lambda$, 0.15λ, 0.2λ. We can find from Fig. 13(a) that the values of $I_z^{\rm wh}(x,0,z=c)$ will decrease rapidly with the increase of z. Figure 13(b) shows the transverse distributions of $I_z^{\rm ev}$, $I_z^{\rm pr}$, $I_z^{\rm co}$, and their overlapping $I_z^{\rm wh}$ as $R=0.1\lambda$ and $z=0.1\lambda$. We can find from Figs. 9 and 13 that the maximal value of $I_z^{\rm wh}(x,0,z=c)$ is much smaller than one of $I_x^{\rm wh}(x,0,z=c)$ for the same values of R and z. For example, maximal values of $I_x^{\rm wh}(x,0,z=c)$ and $I_z^{\rm wh}(x,0,z=c)$ are 0.133 and 0.000817 for $R=0.1\lambda$ and $z=0.1\lambda$ respectively, and the difference is about 162.8 times. Maximal values of $I_x^{\rm wh}(x,0,z=c)$ and $I_z^{\rm wh}(x,0,z=c)$ are 0.058 and 0.000334 for $R=0.1\lambda$ and $z=0.5\lambda$ respectively, and the difference is about 173.7 times. Maximal values of $I_x^{\rm wh}(x,0,z=c)$ and $I_z^{\rm wh}(x,0,z=c)$ are 2.71 and 0.00424 for $R=1.0\lambda$ and $z=1.0\lambda$ respectively, and the difference is about 639.2 times. So the maximal amplitude of intensity distribution of the whole field of the z polarization is much smaller than that of the x polarization and can be neglected.

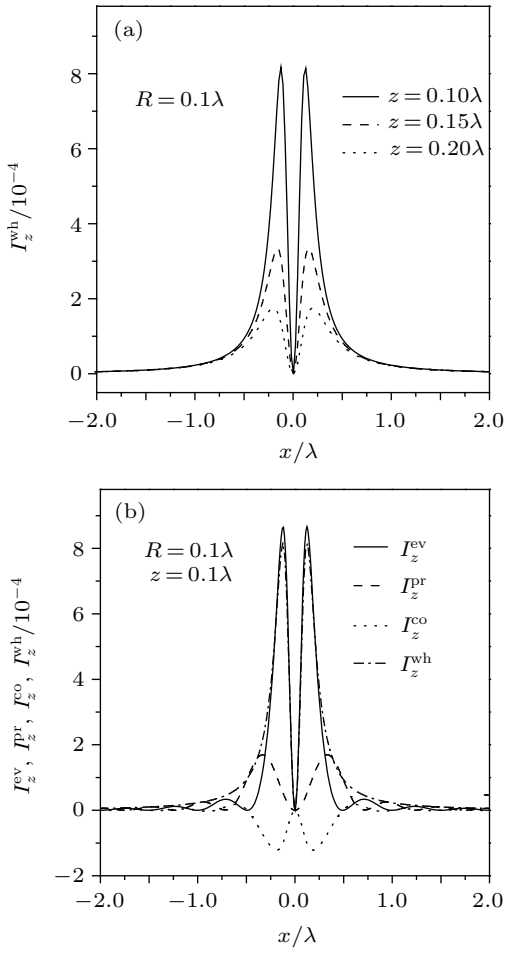


Fig. 13. (a) Transverse distributions of the normalized intensity of the whole field $I_z^{\rm wh}(x,0,z)$ of the z polarization in the x direction as $R=0.1\lambda$ and $z=0.1\lambda$ 0.15λ 0.2λ; (b) the transverse distributions of $I_z^{\rm ev}$, $I_z^{\rm pr}$, $I_z^{\rm co}$, and their overlapping $I_z^{\rm wh}$ as $R=0.1\lambda$ and $z=0.1\lambda$.

Therefore, intensities of the z polarization (the longitudinal electric field) are much smaller than ones of the x polarization (the transverse electric field), and we can think that the longitudinal electric field vanishes and the transverse electric field is treated as the whole electric field.

4. Power transmission function

Since we have supposed that the amplitude of incident plane wave is 1, we can define the amount of incident power at the circular aperture as $P=\pi R^2$. If we then integrate the intensity of the x polarization in the plane z=constant, we can derive the amount of transmitted power. So we can define the power transmission function T of the aperture by the ratio of the amount of transmitted power to P_0.[8] The power transmission functions $T_x^{\rm ev}(z)$ and $T_x^{\rm pr}(z)$ of evanescent wave and propagating field of the x polarization can be given respectively, by

$$T_x^{\rm ev}(z)=\frac{P_x^{\rm ev}}{P_0}=\frac{1}{\pi R^2}\int_{-\infty}^{\infty}\int_{-\infty}^{\infty}I_x^{\rm ev}(x,y,z)\,{\rm d}x\,{\rm d}y, \quad (13a)$$

$$T_x^{\rm pr}(z)=\frac{P_x^{\rm pr}}{P_0}=\frac{1}{\pi R^2}\int_{-\infty}^{\infty}\int_{-\infty}^{\infty}I_x^{\rm pr}(x,y,z)\,{\rm d}x\,{\rm d}y, \quad (13b)$$

According to Eqs. (7)–(13), the dependences of the power transmission functions $T_x^{\rm ev}(z)$ and $T_x^{\rm pr}(z)$ on z for different values of R are calculated, and results are shown in Figs. 14(a) and 14(b), respectively. We can find from Fig. 14(a) that the power transmission function $T_x^{\rm ev}(z)$ decreases rapidly with the increase of z and the attenuation distance is very small and typically smaller than 0.3λ, which is consistent with the evolving of the on-axis evanescent intensity. Taking $z=0.001\lambda$, we find that $T_x^{\rm ev}(z)$ are 1.05 for $R=0.05\lambda$ and 1.46 for $R=0.1\lambda$ respectively, which shows an abnormal transmission due to the very small aperture.

We can find from Fig. 14(b) that power transmission function $T_x^{\rm pr}(z)$ first increases to a maximal value and then decreases with the increase of z as $R=0.2\lambda$ and 0.4λ and the larger the radius R, the less the value will decrease. While the power transmission function $T_x^{\rm pr}(z)$ increases to the a maximal value

and then nearly keeps this value with the increase of z as $R = 0.6\lambda$, 0.8λ, and 1.0λ. We can also find from Fig. 14(b) that the steady power transmission function $T_x^{\rm pr}(z)$ increases with the increase of R, and the steady value of $T_x^{\rm pr}(z)$ can reach 0.9 as $R = 1.0\lambda$ and has nearly no change with the increase of z.

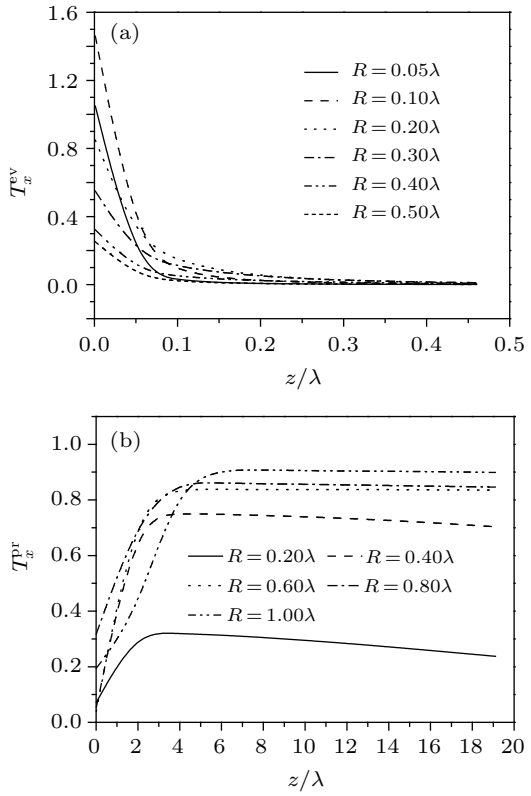


Fig. 14. Dependences of power transmission functions $T_x^{\rm ev}(z)$ (a) and $T_x^{\rm pr}(z)$ (b) on z for different values of R.

5. Conclusion

In this paper, to the best of our knowledge, the analytical nonparaxial vectorial electric field expressions including evanescent and propagating components for both Gaussian beams and plane waves diffracted through a circular aperture are obtained for the first time. Their intensity prosperities and power transmission functions of the diffraction through a circular subwavelength-size aperture are investigated in detail.

It is shown that the evanescent field plays a key role for a small aperture radius (such as $R \leq 0.2\lambda$) in the near-field region (such as several 0.1λ). The intensity of the evanescent field decreases rapidly with the increase of z and the attenuation distance is very small, typically a fraction of wavelength λ, which is consistent with the evolution of the power transmission function of the evanescent field with the increase of z. When R increases, the whole intensity is complicated and determined by all components. When the radius R becomes larger (for example, $R \geq 0.3\lambda$), the propagating field will play a more important role. The propagating field can propagate larger distance z with the increase of R, and the value of steady power transmission function of the propagating field of the x polarization can reach 0.9 as $R = 1.0\lambda$ and has nearly no change with the increase of z. So the propagating field plays a key role for a large radius (such as $R \geq 1.0\lambda$) in the near- and far-field regions (for example, $R \geq 0.1\lambda$).

It is shown that the transverse distribution of the x polarization is axially symmetric while the transverse distribution of the z polarization is always 0 as $x = 0$, and intensities of the z polarization are much smaller than ones of the x polarization and can be neglected. The transverse distribution of the intensity of the propagating field of the x polarization can be converted from a non-Gaussian mode distribution to a Gaussian one with the propagation of light for a larger radius (for example $R \geq 0.4\lambda$).

Our study can be helpful for understanding the essence of diffraction at a subwavelength aperture and the relationship between evanescent and propagating components in the near-field region,[21] and be applied to apertured near-field scanning optical microscopy.

References

[1] Rayleigh L 1897 *Philos. Mag.* **43** 259
[2] Bethe H A 1944 *Phys. Rev.* **66** 163
[3] Bekefi G 1953 *J. Appl. Phys.* **24** 1123
[4] Mitrofanov O, Lee M, Hsu J W P, Pfeifer L N, West K W, Wynn J D and Federici J F 2001 *Appl. Phys. Lett.* **79** 907
[5] Hsu W and Barakat R 1994 *J. Opt. Soc. Am.* A **11** 623
[6] Lü B and Duan K 2003 *Opt. Lett.* **28** 2440
[7] Gillen G D, Baughman K and Guha S 2009 *Opt. Express* **17** 1478
[8] Guha S and Gillen G D 2005 *Opt. Express* **13** 1424
[9] Gillen G D, Guha S and Christandl K 2006 *Phys. Rev.* A **73** 013409
[10] Zhou G 2008 *Opt. Express* **16** 3504
[11] Duan K and Lü B 2003 *Opt. Express* **11** 1474
[12] Gillen G D and Guha S 2004 *Am. J. Phys.* **72** 1195
[13] Carter W H 1972 *J. Opt. Soc. Am.* **62** 1195
[14] Agrawal G P and Pattanayak D N 1979 *J. Opt. Soc. Am.* **69** 575
[15] Zhou G 2006 *Opt. Lett.* **31** 2616
[16] Guo H, Chen J and Zhuang S 2006 *Opt. Express* **14** 2095
[17] Zhou G, Ni Y and Zhang Z 2007 *Opt. Commun.* **272** 32
[18] Deng D and Guo Q 2007 *Opt. Lett.* **32** 2711
[19] Wu G, Lou Q and Zhou J 2008 *Opt. Express* **16** 6417
[20] Wang Z, Zhou M, Zhang W, Zhou Y, Cao G and Gao C 2011 *J. Opt.* **13** 055704
[21] Pu X Y, Jiang N, Han D Y, Feng Y L and Ren Y T 2010 *Chin. Phys.* B **19** 054207